Supplementary Material

Higher-Order Band Topology in Twisted Moiré Superlattice

Bing Liu[1], Lede Xian[2], Haimen Mu[1], Gan Zhao[1], Zhao Liu[1], Angel Rubio[2,3,4], and Z. F. Wang[1,*]

[1]*Hefei National Laboratory for Physical Sciences at the Microscale, CAS Key Laboratory of Strongly-Coupled Quantum Matter Physics, Department of Physics, University of Science and Technology of China, Hefei, Anhui 230026, China*
[2]*Max Planck Institute for the Structure and Dynamics of Matter, Center for Free Electron Laser Science, Luruper Chaussee 149, 22761 Hamburg, Germany*
[3]*Center for Computational Quantum Physics, Simons Foundation Flatiron Institute, New York, NY 10010 USA*
[4]*Nano-Bio Spectroscopy Group, Departamento de Fisica de Materiales, Universidad del País Vasco, UPV/EHU-20018 San Sebastián, Spain*

*Correspondence to: zfwang15@ustc.edu.cn

1. Tight-Binding Hamiltonian

The TB Hamiltonian is described by the single p_z-orbital model as

$$H = \sum_i \varepsilon_i c_i^\dagger c_i + \sum_{ij} t_{ij} c_i^\dagger c_j \tag{S1}$$

where ε_i is the on-site energy and t_{ij} is hopping parameter between i-site and j-site. The hopping parameter can be expressed as[1,2]

$$t_{ij} = V_\sigma (\frac{\boldsymbol{d}\cdot\hat{\mathrm{z}}}{d})^2 + V_\pi [1-(\frac{\boldsymbol{d}\cdot\hat{\mathrm{z}}}{d})^2] \tag{S2}$$

where $V_\sigma = V_\sigma^0 \mathbf{e}^{-(d-d_c)/\delta_0}$ and $V_\pi = V_\pi^0 \mathbf{e}^{-(d-a_0)/\delta_0}$. d and $\boldsymbol{d}$ is the distance and position-vector between i-site and j-site, respectively. For the TBG, ε_i = 0 eV, V_σ^0 = 0.48 eV, V_π^0 = –2.7 eV, $\delta_0 = 0.184\sqrt{3}a_0$, a_0=1.42Å, d_c=3.35Å. For the TBBN, ε_i = 1.9 eV for B and –1.9 eV for N, V_σ^0 = 0.48 eV, V_π^0 = 3.24 eV, $\delta_0 = 0.184\sqrt{3}a_0$, a_0=1.45Å, d_c=3.33Å. In our calculations, the intralayer hopping parameter is limited between two nearest-neighbor sites, while the interlayer hopping parameter is limited between two sites with d < 6.0Å. This TB Hamiltonian can

reproduce the main band feature calculated by first-principles calculations. Moreover, the bulk topological index obtained from this TB Hamiltonian is also consistent with that obtained from the first-principles calculations, directly identifying the validity of our TB model (see Fig. S6 and Fig. S7).

2. Structure Relaxation

Due to the mismatch between top and bottom twisted layers, a moiré superlattice is formed, where different local stacking patterns (AA, AB or BA) appear periodically. The commensurate twist-angle is determined by the condition[3] $\cos(\theta) = (3n^2 + 3n + 1/2)/(3n^2 + 3n + 1)$, where n is an integer. The interlayer distance is variable in real-space, so the classical molecular dynamics simulations implemented in LAMMPS[4] is performed to relax the moiré superlattice. All atoms are relaxed until the forces are smaller than 0.001 eV/ Å.

3. First-Principles Calculations

Based on the density functional theory (DFT), the first-principles calculations are carried out in the framework of generalized gradient approximation with Perdew-Burke-Ernzerhof functional using the Vienna Ab initio simulation package (VASP)[5]. All calculations are performed with a plane-wave cutoff of 520 eV on the 3×3×1 Monkhorst-Pack k-point mesh. The vacuum layer of 20 Å thick is used to ensure decoupling between neighboring slabs.

4. Double Band Inversion

Recently, a new kind of topological index (quantized fractional corner charge) is proposed to distinguish the rotation symmetry protected higher-order topological state with vanishing polarization[6]. Within this framework, the C_{6z} and C_{3z} symmetry protected 2D SOTI can be characterized by the topological index Q as:

$$C_{6z} \rightarrow Q = [\mathrm{M}_1^{(2)}]/4 + [\mathrm{K}_1^{(3)}]/6 \quad \mathrm{mod} \quad 1 \tag{S3}$$

$$C_{3z} \rightarrow Q = [\mathrm{K}_2^{(3)}]/3 \quad \mathrm{mod} \quad 1 \tag{S4}$$

where

$$[\Pi_p^{(n)}] = \#\Pi_p^{(n)} - \#\Gamma_p^{(n)} \tag{S5}$$

Eq. S5 denotes the occupied band-number difference for C_{nz} symmetry with eigenvalue $\exp[2\pi i(p-1)/n]$ (p=1, 2 ... n) between the high-symmetric k-point Π and Γ. In the main text, we have shown that the topological index Q is nonzero for both TBG and TBBN, demonstrating a nontrivial higher-order band topology. It's well known that the nontrivial Z_2 index described conventional first-order 2D and 3D topological insulators can be understood in an intuitive physical picture, called the band inversion. Here, we found that the topological index Q described 2D SOTI for TBG and TBBN can be understood in a similar way, called the double band inversion. Recently, the same mechanism has also been reported for the higher-order topological state in the Bismuth[7]. In the following part, we will give a detailed analysis about this mechanism.

The polarization of TBG with C_{6z} symmetry is always zero, satisfying the prerequisite for the topological index Q. The definition of Q has two terms in Eq. S3, we will consider them one by one. Since the $C_{2z}T$ symmetry protected Stiefel-Whitney number (ω) has also been used to characterize the bulk topology of TBG[8], the calculated ω_1=0 and ω_2=1 in the two high-energy gaps of TBG indicates that[9]

$$[\mathrm{M}_2^{(2)}] = \#\mathrm{M}_2^{(2)} - \#\Gamma_2^{(2)} = \text{even} \tag{S6}$$

Since $[\mathrm{M}_1^{(2)}]$ ($[\mathrm{M}_2^{(2)}]$) denotes the occupied band-number difference for C_{2z} symmetry with eigenvalue +1(–1) between M and Γ point, their summation will satisfy

$$[\mathrm{M}_1^{(2)}] + [\mathrm{M}_2^{(2)}] = 0 \tag{S7}$$

Combining Eq. S6 and S7, we found that

$$[\mathrm{M}_1^{(2)}] = \text{even} \tag{S8}$$

Combining Eq. S3 and S8, we will obtain the condition for nonzero value of Q as

$$Q\begin{cases} = 0, & [\mathrm{M}_1^{(2)}] = 4,8,12\cdots \\ \neq 0, & [\mathrm{M}_1^{(2)}] = 2,6,10\cdots \end{cases} \tag{S9}$$

Eq. S9 indicates that if one wants to tune Q from zero to nonzero, at least a double band

inversion is needed. The character table of TBG (space group 177) is shown in Table 1(a). At Γ point, the band for C_{2z} symmetry with eigenvalue +1 is single- or double-degenerate. At M point, the band for C_{2z} symmetry with eigenvalue +1 is only single-degenerate. Therefore, the double band inversion can be realized by inverting a double-degenerate-band at Γ point, or by inverting two single-degenerate-bands with the same eigenvalue at Γ and M point simultaneously.

Next, we turn to the second term of the topological index Q in Eq. S3. Due to the C_{6z} symmetry of TBG, we have

$$\#\mathrm{K}_p^{(3)} = \#\mathrm{K}_p'^{(3)}, \qquad p = 1,2,3 \tag{S10}$$

where K and K′ are two nonequivalent K points, and $\#\mathrm{K}_p^{(3)}$ denotes the occupied band-number for C_{3z} symmetry with eigenvalue $\exp[2\pi i(p-1)/3]$. Moreover, due to the time-reversal symmetry, we also have

$$\#\mathrm{K}_2^{(3)} = \#\mathrm{K}_3'^{(3)} \tag{S11}$$

Combining Eq. S10 and S11, one obtains

$$\#\mathrm{K}_2^{(3)} = \#\mathrm{K}_3^{(3)} \tag{S12}$$

Similar to Eq. S7, we have the following relation

$$[\mathrm{K}_1^{(3)}] + [\mathrm{K}_2^{(3)}] + [\mathrm{K}_3^{(3)}] = 0 \tag{S13}$$

where $[\mathrm{K}_1^{(3)}]$ ($[\mathrm{K}_2^{(3)}], [\mathrm{K}_3^{(3)}]$) denotes the occupied band-number difference for C_{3z} symmetry with eigenvalue +1 ($\exp(i2\pi/3)$, $\exp(i4\pi/3)$) between K and Γ point. Combining Eq. S12 and S13, we found that

$$[\mathrm{K}_1^{(3)}] + 2[\mathrm{K}_2^{(3)}] = 0 \tag{S14}$$

Therefore

$$[\mathrm{K}_1^{(3)}] = \text{even} \tag{S15}$$

Combining Eq. S3 and S15, we will obtain the condition for nonzero value of Q as

$$Q\begin{cases}=0, & [\mathrm{K}_1^{(3)}]=6,12,18\cdots \\ \neq 0, & [\mathrm{K}_1^{(3)}]=2,4,8\cdots \end{cases} \tag{S16}$$

Eq. S16 indicates that if one wants to tune Q from zero to nonzero, at least a double band inversion is needed. As shown in Table 1(a), the band for C_{3z} symmetry with eigenvalue +1 is single-degenerate at Γ and K points. Therefore, the double band inversion can be realized by inverting two single-degenerate-bands with the same eigenvalue at Γ and K point simultaneously.

Lastly, the analysis for C_{3z} symmetry protected topological index Q in Eq. S4 is similar to the above process if the related polarization is zero, we will obtain the condition for nonzero value of Q as

$$Q\begin{cases}=0, & [\mathrm{K}_2^{(3)}]=3,6,9\cdots \\ \neq 0, & [\mathrm{K}_2^{(3)}]=1,2,4\cdots \end{cases} \tag{S17}$$

Eq. S17 indicates that if one wants to tune Q from zero to nonzero, at least a single band inversion is needed. The character table of TBBN (space group 150) is shown in Table 1(b). The bands for C_{3z} symmetry with eigenvalue $\exp(i2\pi/3)$ and $\exp(i4\pi/3)$ are degenerate at both Γ and K points, forming a double-degenerate-band with different eigenvalues. However, only the eigenvalue $\exp(i2\pi/3)$ is accounted for the topological index Q. Therefore, the two bands are inverted but the effective inverted component is only one band. Here, we still call it the double band inversion to make it consistent with the case of C_{6z} symmetry.

5. Domain-Wall State

Along the rotation-invariant line preserving the C_{2y} symmetry in the first Brillouin zone of TBG, the rotation winding number is well defined, which is $\nu_{\pm}=1$ for each rotation sector with eigenvalue $C_{2y}=\pm 1$.[10] Physically, the nonzero rotation winding number will induce a pair of helical edge states on rotation symmetric boundary in TBG, propagating along opposite directions in each rotation sector. If the boundary of TBG is incompatible with C_{2y} symmetry, the corresponding helical edge states will be gapped by a mass-term, otherwise, they are still gapless. For the rhombus TBG cluster studied in our work, the edges are gapped as the

boundary does not consistent with C_{2y} symmetry, and the mass-term vanishes at the C_{2y} symmetric corners. Therefore, in the basis of the gapless helical edge states, the effective edge Hamiltonian and two rotation symmetries can be written as $H=k\sigma_z$, $C_{2x}=\sigma_x$ and $C_{2y}=\sigma_y$. Consequently, the symmetry allowed mass-term will be $m\sigma_x$, which is incompatible with H and C_{2y}. At the 120° corner of TBG, the two gapped edges are connected by C_{2y} symmetry. Since $C_{2y}(m\sigma_x)\ C_{2y}^{-1}=-m\sigma_x$, the mass sign is inverted crossing the 120° corner, forming a domain wall at the corner and resulting in the in-gap corner states. Similarly, at the 60° corner of TBG, the two gapped edges are connected by C_{2x} symmetry. Since $C_{2x}(m\sigma_x)\ C_{2x}^{-1}=m\sigma_x$, the mass sign is not inverted crossing the 60° corner. Therefore, there is no in-gap corner states.

Therefore, the Hamiltonian of two gapped topological edge states on 120° corner of TBG can be written as

$$\begin{aligned} H_1 &= k\sigma_z + m\sigma_x \\ H_2 &= k\sigma_z - m\sigma_x \end{aligned} \tag{S18}$$

where m is the mass-term, as shown in Fig. S2(a). We can solve Eq. S18 by discretizing it to a one-dimensional lattice model. The mass-term is inverted crossing the 120° corner. The corresponding discrete energy-levels of Eq. S18 is shown in Fig. S2(b). Obviously, there are two degenerate in-gap states at the zero-energy. The spatial distribution of this in-gap state is shown in the inset of Fig. S2(b), which is localized at the corner region, exhibiting the characterized feature of a domain-wall state. Similarly, the Hamiltonian of two gapped topological edge states on 60° corner of TBG can be written as [Fig. S2(c)]

$$\begin{aligned} H_1 &= k\sigma_z + m\sigma_x \\ H_2 &= k\sigma_z + m\sigma_x \end{aligned} \tag{S19}$$

The mass-term is not inverted crossing the 60° corner. Therefore, there is no in-gap domain-wall states at the zero-energy, as shown in Fig. S2(d).

To explore the transport properties of the gapped edge states crossing the corner, based on the above discretized one-dimensional lattice model, we present a NEGF calculation, where a linear mass inversion is used in the scattering region (corner region), as shown in Fig. S5(a).

The calculated conductance (G) and 1/(1-G) as a function of energy (E) and length of scattering region (L) is shown in Fig. S5(b) and S5(c), respectively. For a fix energy above the gap, one can see the periodic conductance oscillation with the increasing length of corner region, demonstrating the feature of resonance-tunneling. Physically, the mass inversion in two gapped edge states will make their wavefunciton mismatch with each other. However, by tuning the length of the corner region, one can control the degree of this mismatch. Generally, if the condition $kL=n\pi$ is satisfied, a resonance-tunneling will be realized, corresponding to the maximum conductance with a best matched wavefunction. Moreover, for a fixed length of L, the conductance of the edge state also varies with the changing energy, which is dramatically different to conventional gapless edge state induced quantized conductance. These behaviors are expected to be detected by the transport measurement, deserving to be investigated in the future works.

6. Twisted Bilayer SiC

Besides TBBN, the twisted bilayer SiC is also confirmed to be a 2D SOTI. For twist-angle θ=7.3°, its band structure and bulk topological index obtained from the DFT calculations is shown in Fig. 8(a) and 8(b), respectively. The nonzero Q in both upper and lower gaps clearly demonstrates a higher-order band topology in these two high-energy gaps, which is comparable to that in TBBN. Additionally, since the low-energy band structure of transition metal dichalcogenide (TMD) is also described by the massive Dirac equation, the twisted TMD is expected to be another big family of higher-order topological materials.

Reference

1. G. Trambly de Laissardière, D. Mayou and L. Magaud, Nano Lett. **10**, 804 (2010).
2. P. Moon and M. Koshino, Phys. Rev. B **87**, 205404 (2013).
3. J. M. B. Lopes dos Santos, N. M. R. Peres and A. H. Castro Neto, Phys. Rev. Lett. **99**, 256802 (2007).
4. S. Plimpton, J. Comp. Phys. **117**, 1 (1995).
5. G. Kresse and J. Furthmüller, Phys. Rev. B **54**, 11169 (1996).
6. W. A. Benalcazar, T. Li and T. L. Hughes, Phys. Rev. B **99**, 245151 (2019).
7. C.-H. Hsu, X. Zhou, T.-R. Chang, Q. Ma, N. Gedik, A. Bansil, S.-Y. Xu, H. Lin and L. Fu, Proc. Natl. Acad. Sci. U.S.A. **116**, 13255 (2019).
8. M. J. Park, Y. Kim, G. Y. Cho and S. Lee, Phys. Rev. Lett. **123**, 216803 (2019).
9. A. Alexandradinata, X. Dai and B. A. Bernevig, Phys. Rev. B **89**, 155114 (2014).
10. M. Kindermann, Phys. Rev. Lett. **114**, 226802 (2015).

(a)

HSP	Irreps	E	C_{2z}	C_{3z}
Γ	A_1	1	1	1
	A_2	1	1	1
	B_1	1	-1	1
	B_2	1	-1	1
	E_2	2	2	-1
	E_1	2	-2	-1
M	A	1	1	/
	B_1	1	1	
	B_2	1	-1	
	B_3	1	-1	
K	A_1	1	/	1
	A_2	1		1
	E	2		-1

(b)

HSP	Irreps	E	C_{3z}
Γ	A_1	1	1
	A_2	1	1
	E	2	-1
K	A_1	1	1
	A_2	1	1
	E	2	-1

Table 1. The character table of (a) TBG and (b) TBBN at different high-symmetric k points.

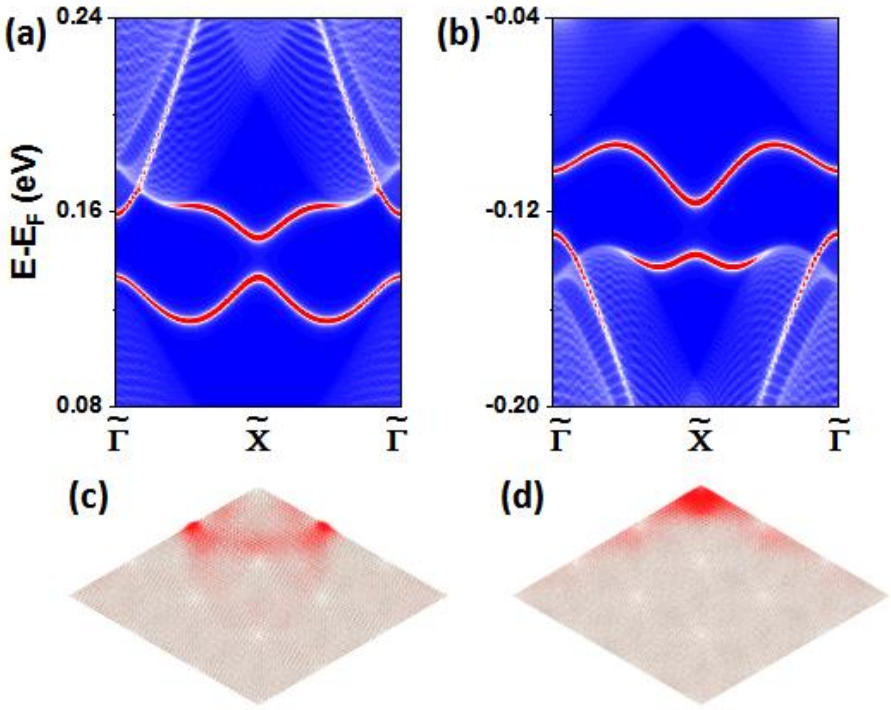

Figure S1: Edge and corner topology of TBG for θ=1.8°. (a) and (b) Semi-infinite spectral function of TBG along the edge cutting through AA-stacking region in the upper and lower gap. (c) and (d) Spatial distribution of in-gap topological corner states around the 120°corner in the upper and lower gap. The circle size denotes the weighting factor of corner states. These results are consistent with those for θ=2.1° in Fig. 3. The structure in (c) and (d) is the corner part of the whole TBG cluster, where only the top region is a real corner.

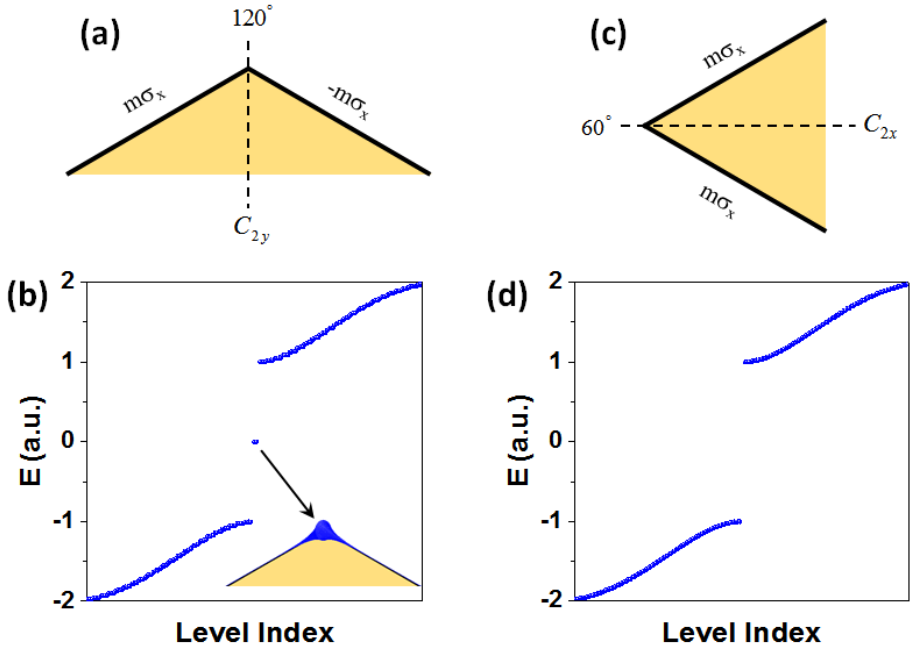

Figure S2: (a) and (c) Mass-term of the topological edge states at 120° and 60° corner of TBG. (b) and (d) Discrete energy-levels of (a) and (c). The inset in (b) is the spatial distribution of the in-gap domain-wall state at zero-energy.

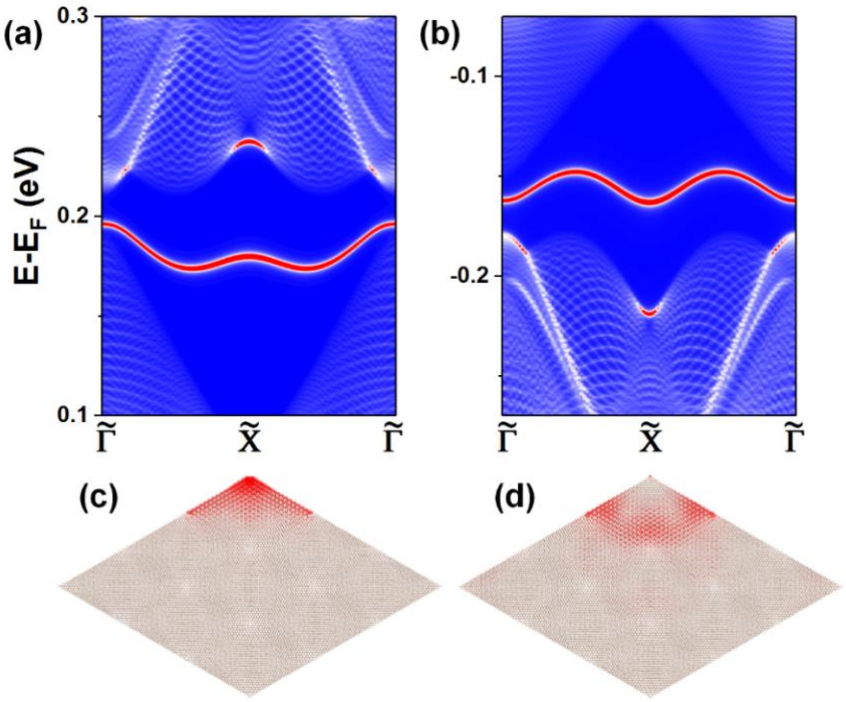

Figure S3: The twist-center of TBG is chosen at single-atom for θ=2.1°. (a) and (b) Semi-infinite spectral function of TBG along the edge cutting through AA-stacking region in the upper and lower gap. (c) and (d) Spatial distribution of in-gap topological corner states around the 120° corner in the upper and lower gap. The circle size denotes the weighting factor of corner states. The structure in (c) and (d) is the corner part of the whole TBG cluster, where only the top region is a real corner.

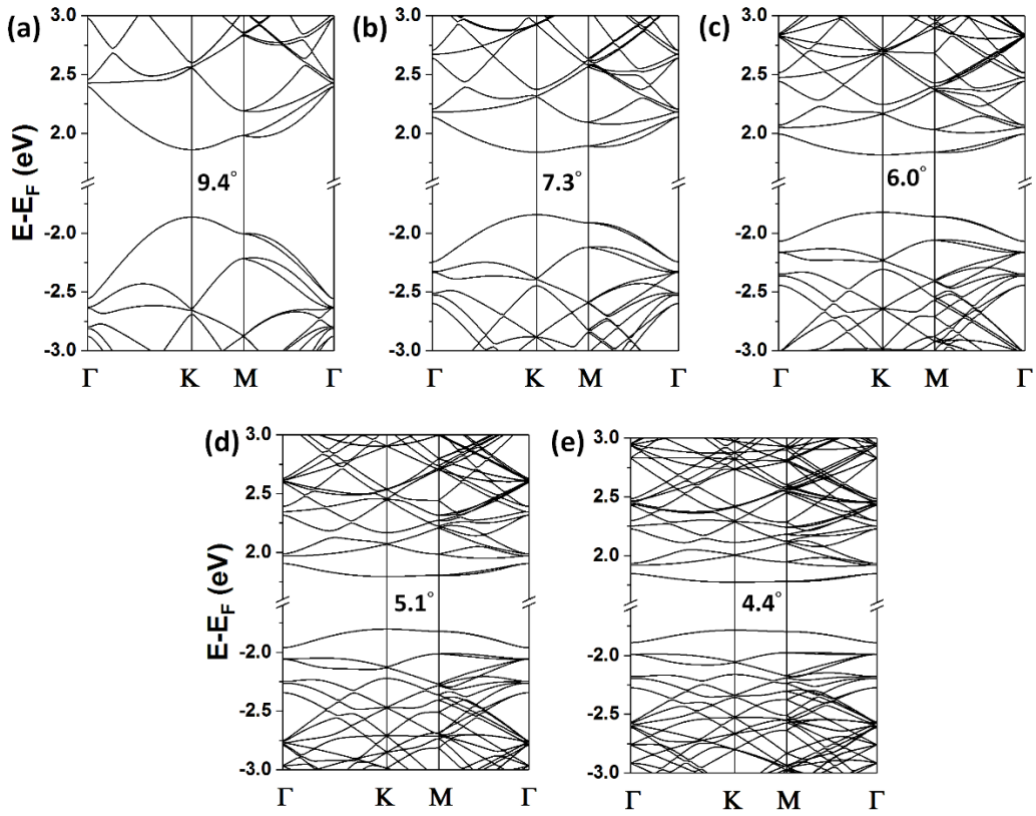

Figure S4: TB band structure of TBBN with different twist-angles. (a) θ=9.4°, (b) θ=7.3°, (c) θ=6.0°, (d) θ=5.1° and (e) θ=4.4°.

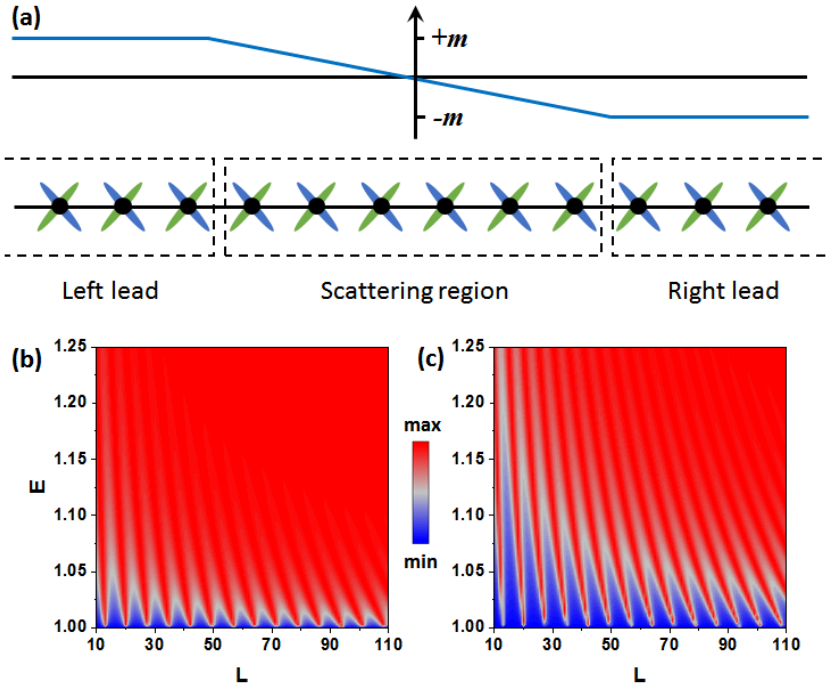

Figure S5: Conductance of the gapped edge state crossing the corner. (a) One dimensional discretized lattice of the edge Hamiltonian. The mass-term (m) is linearly inverted in the center scattering region. Each lattice site has a pseudo-spin degree of freedom denoted by two different colors. The mass-term has the opposite sign in the left and right lead region. (b) Conductance (G) vs. energy (E) and scattering region length (L). L denotes the number of lattice site in the scattering region. m=1 is used in our calculations. (c) To show the conduction oscillation more clearly at higher energy, 1/(1-G) vs. E and L is plotted.

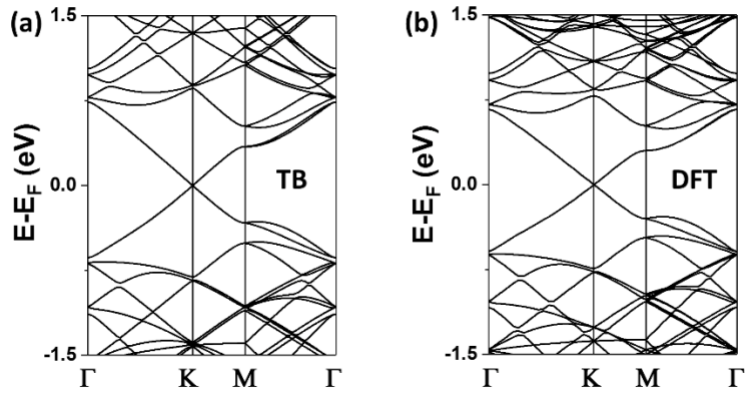

(c)

TB	$\#\Gamma_1^{(2)}$	$\#M_1^{(2)}$	$\#\Gamma_1^{(3)}$	$\#K_1^{(3)}$	$[M_1^{(2)}]$	$[K_1^{(3)}]$	Q
Δ_{up}	129	127	88	84	-2	-4	5/6
Δ_{low}	127	125	84	84	-2	0	1/2

(d)

DFT	$\#\Gamma_1^{(2)}$	$\#M_1^{(2)}$	$\#\Gamma_1^{(3)}$	$\#K_1^{(3)}$	$[M_1^{(2)}]$	$[K_1^{(3)}]$	Q
Δ_{up}	513	507	342	338	-6	-4	5/6
Δ_{low}	511	505	338	338	-6	0	1/2

Figure S6: (a) and (b) TB and DFT band structure of TBG for θ=5.1˚. (c) and (d) TB and DFT bulk topological index of TBG for θ=5.1˚. $\#\Gamma_1^{(2)}$ ($\#M_1^{(2)}$) denotes the band number below the energy gap for C_{2z} symmetry with eigenvalue 1 at Γ (M) point. $\#\Gamma_1^{(3)}$ ($\#K_1^{(3)}$) denotes the band number below the energy gap for C_{3z} symmetry with eigenvalue 1 at Γ (K) point. $[M_1^{(2)}]=\#M_1^{(2)}-\#\Gamma_1^{(2)}$, $[K_1^{(3)}]=\#K_1^{(3)}-\#\Gamma_1^{(3)}$ and $Q=[M_1^{(2)}]/4+[K_1^{(3)}]/6$ mod 1

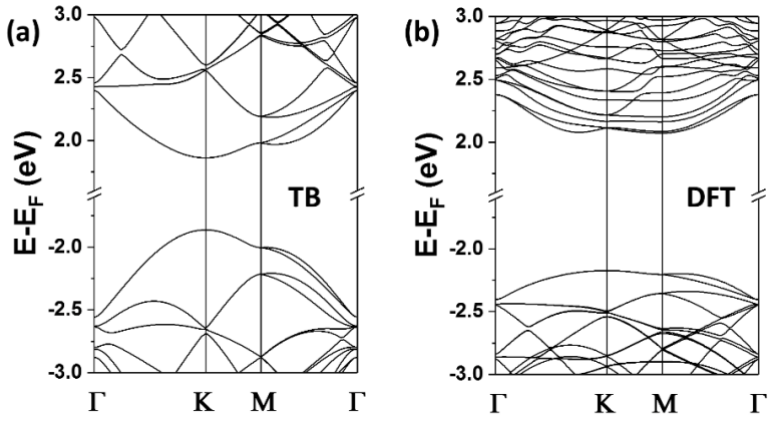

(c)

TB	$\#\Gamma_2^{(3)}$	$\#K_2^{(3)}$	$[K_2^{(3)}]$	Q
Δ_{up}	25	26	1	1/3
Δ_{low}	23	24	1	1/3

(d)

DFT	$\#\Gamma_2^{(3)}$	$\#K_2^{(3)}$	$[K_2^{(3)}]$	Q
Δ_{up}	99	100	1	1/3
Δ_{low}	97	98	1	1/3

Figure S7: (a) and (b) TB and DFT band structure of TBBN for θ=9.4°. (c) and (d) TB and DFT bulk topological index of TBBN for θ=9.4°. $\#\Gamma_2^{(3)}$ ($\#K_2^{(3)}$) denotes the band number below the energy gap for C_{3z} symmetry with eigenvalue exp(i2π/3) at Γ (K) point. $[K_2^{(3)}]= \#K_2^{(3)}–\#\Gamma_2^{(3)}$, and $Q= [K_2^{(3)}]/3$ mod 1

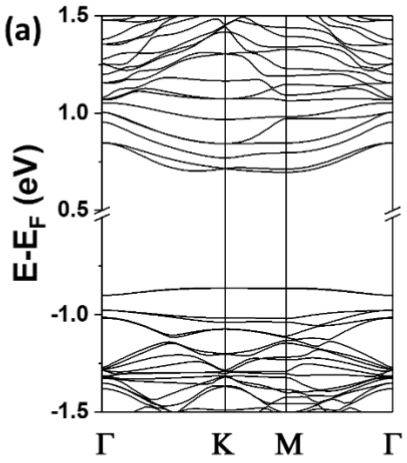

(b)

DFT	$\#\Gamma_2^{(3)}$	$\#K_2^{(3)}$	$[K_2^{(3)}]$	Q
Δ_{up}	163	164	1	1/3
Δ_{low}	161	162	1	1/3

Figure S8: (a) DFT band structure of twisted bilayer SiC for θ=7.3°. (b) DFT bulk topological index of twisted bilayer SiC for θ=7.3°. The labels have the same meaning as those in Fig. S7.